Microbial strong organic ligand production is tightly coupled to iron in hydrothermal plumes

Colleen L. Hoffman[1,2,3*†] and Patrick J. Monreal[3,4*†], Justine B. Albers[5], Alastair J.M. Lough[6], Alyson E. Santoro[5], Travis Mellett[3,7], Kristen N. Buck[7,8], Alessandro Tagliabue[9], Maeve C. Lohan[6], Joseph A. Resing[1,2,3], Randelle M. Bundy[3]

[1]Joint Institute for the Study of Atmosphere and Ocean, University of Washington, 3737 Brooklyn Avenue NE, Seattle, WA 98195, USA

[2]Cooperative Institute for Climate, Ocean, and Ecosystem Studies, University of Washington, 3737 Brooklyn Avenue NE, Seattle, WA 98195, USA

[3]School of Oceanography, University of Washington, 1501 NE Boat Street, Seattle, WA 98195, USA

[4]Earth Systems Program, Stanford University, 473 Via Ortega, Stanford, CA 94305, USA

[5]Department of Ecology, Evolution, and Marine Biology, University of California, Santa Barbara, CA 93106, USA

[6]Department of Ocean and Earth Sciences, National Oceanography Centre, University of Southampton, European Way, Southampton SO14 3ZH, United Kingdom

[7]College of Marine Science, University of South Florida, 140 7th Avenue South, St. Petersburg, FL, 33701, USA

[8]College of Earth, Ocean, and Atmospheric Sciences, Oregon State University, 2651 SW Orchard Ave, Corvallis, OR, 97331, USA

[9]Department of Earth, Ocean, and Ecological Sciences, University of Liverpool, 4 Brownlow Street, Liverpool l69 3GP, United Kingdom

†These authors contributed equally and are co-first authors

*Correspondence: Colleen L. Hoffman and Patrick J. Monreal

Email: clhoffma@gmail.com, pmonreal@uw.edu

Abstract. Hydrothermal vents have emerged as important sources of iron to seawater, yet only a subset of this iron is soluble and persists long enough to impact the deep ocean iron inventory. The longevity and solubility of iron in seawater is in part governed by strong organic ligands that are produced by microorganisms and are a part of the ocean's dissolved organic iron-binding ligand pool. Organic ligands have long been recognized to support elevated dissolved iron in hydrothermal vent plumes. Siderophores are one group of microbially-produced organic ligands that have especially high binding affinities for iron. Here we present the first direct measurements of siderophore concentrations in hydrothermal vents, which we compare to bulk strong iron-binding ligand concentrations, along a 1,700 km section of the Mid-Atlantic Ridge. Siderophores were found in hydrothermal plumes at all sites, with proximity to the vent playing an important role in dictating siderophore type and diversity. The notable presence of amphiphilic siderophores may point to microbial utilization of siderophores to access particulate hydrothermal iron, and the exchange of dissolved and particulate iron. The tight coupling between strong ligands and dissolved iron within neutrally buoyant plumes across distinct hydrothermal environments, and the presence of dissolved siderophores with siderophore-producing microbial genera, suggests that biological production of ligands influences iron chemistry in hydrothermal systems.

1. Introduction

Over the last few decades, observations and modelling efforts have increased our understanding about the critical role organic ligands play in the cycling, transport, and utilization of trace metals (Tagliabue et al., 2017; Buck et al., 2018; Bundy et al., 2018; Moore et al., 2021; Hawkes et al., 2013b; Kleint et al., 2016). Iron (Fe) binding organic ligands in seawater have a wide range of sources, which are only just beginning to be understood. Recent observations suggest that microbial production of siderophores, humic-like substances and exopolysaccharides are some of the major contributors of marine organic ligands (Hassler et al., 2017), and microbial production and alteration of ligands influences Fe cycling in environments ranging from hydrothermal plumes (Cowen and Bruland, 1985; Cowen et al., 1990) to the open ocean (Lauderdale et al., 2020; Whitby et al., 2024, 2020; Misumi et al., 2013). Strong Fe-binding organic ligands (defined as L_1 ligands) are a heterogeneous mixture of microbially produced compounds that are operationally classified based on their binding strength with Fe (defined as $\log K^{cond}_{Fe',FeL} > 12$). They are thermodynamically favored to complex and stabilize external sources of Fe to prevent its scavenging and removal (Fishwick et al., 2014; Aguilar-Islas et al., 2010).

Siderophores are the strongest known Fe-binding organic ligands. They are produced by bacteria and fungi to facilitate Fe uptake and solubilize otherwise inaccessible phases in the marine environment (Butler, 2005; Manck et al., 2022). They have primarily been considered an important microbial strategy for Fe acquisition in the low dissolved Fe (dFe) surface ocean (Vraspir and Butler, 2009; Butler, 2005). However, siderophore uptake and biosynthesis genes were observed in >70% of Fe-related bacterial transcripts in a hydrothermal

environment in Guaymas Basin (Li et al., 2014), have been identified in oxygen-deficient zones (Moore et al., 2021), and are a common Fe acquisition strategy within terrestrial and pathogenic ecosystems (Sandy and Butler, 2009), all of which are environments where Fe concentrations are orders of magnitude higher than surface seawater.

Previous studies have examined total concentrations of Fe-binding ligands in hydrothermal plumes and throughout the deep ocean (Sander and Koschinsky, 2011; Hawkes et al., 2013b; Mahieu et al., 2024; Buck et al., 2018; Kleint et al., 2016), as well as siderophores observed below the euphotic zone (Park et al., 2023; Boiteau et al., 2019; Bundy et al., 2018; Moore et al., 2021). A 'stabilizing agent' has been proposed for the long-range transport of hydrothermal dFe into the ocean interior, which has been hypothesized to be inorganic colloids (Fitzsimmons et al., 2017; Fitzsimmons and Boyle, 2014; Yücel et al., 2011; Lough et al., 2019), organic ligands including strong ligands and weaker ligands (Hawkes et al., 2013b; Mahieu et al., 2024; Kleint et al., 2016; Hassler et al., 2020; Slagter et al., 2019), or a combination of the two. The role of strong Fe-binding ligands in hydrothermal dFe transport represents an important knowledge gap in how hydrothermal vents may impact the ocean dFe inventory (Resing et al., 2015) and how siderophores may influence Fe transformations in hydrothermal plumes. While genetic evidence suggests that siderophore cycling may occur in hydrothermal systems (Li et al., 2014), no previous studies have ever directly measured siderophores in hydrothermal systems due to the high sample volume requirements, difficulty in obtaining deep ocean trace metal samples, and the time-intensive nature of the analyses. Here, for the first time, we identified siderophores and siderophore-producing microbes in 11 geochemically distinct hydrothermal plume environments along the slow-spreading (20-50 mm/yr) Mid-Atlantic Ridge (MAR). Four black smokers (high temperature, high Fe), four off-axis sites, one diffuse vent (low temperature, low Fe), one alkaline vent (pH 9-11, very low Fe), and one non-vent fracture zone were investigated using both competitive ligand exchange-adsorptive cathodic stripping voltammetry and state-of-the-art liquid chromatography coupled to electrospray ionization mass spectroscopy (Boiteau et al., 2016) in a targeted approach to search for known siderophores and possible compounds present in the L_1 ligand pool in hydrothermal plumes. Microbial community analysis was also compared at three sites to understand whether siderophore production impacts Fe transformation in hydrothermal plumes.

2. Results and Discussion

2.1 The role of iron-binding ligands in hydrothermal plumes

Strong Fe-binding ligands (L_1) have previously been found in neutrally-buoyant hydrothermal plumes across a variety of systems (Wang et al., 2022; Bennett et al., 2008; Tagliabue et al., 2017; Hawkes et al., 2013b; Resing et al., 2015; Buck et al., 2018). However, the relationship between organic ligands and dFe have never been investigated together systematically across a wide variety of vents in the same study. In this work, the average binding strength and concentration of organic Fe-binding ligands were quantified in 11 vent systems that spanned a wide range in dFe concentrations (0.41-90 nM) and underlying vent geology. Over 99% of

dFe in the neutrally buoyant plume samples were complexed by L_1 ligands and the ligands were almost always completely saturated with dFe, meaning Fe-free 'excess' L_1 ligands capable of binding additional Fe were present in low concentrations (< 1 nM; **Fig. S1**). As a result, dFe concentrations were tightly coupled to L_1 ligands in a nearly 1:1 ratio (**Fig. 1d**), similar to previous studies in other neutrally buoyant plumes (**Fig. 1e**) (Buck et al., 2015, 2018).

The strong coupling between dFe and ligands was only observed at sites where L_1 ligands were detected. Some samples, that were closer to the buoyant plume and vent source, contained high concentrations of weaker ligands ($\log K^{cond}_{Fe',FeL} < 12$, **Table S2-S3**) whose concentrations had no correlation with dFe. This is consistent with these environments likely being dominated by complex Fe phases, which could include various inorganic forms (e.g. nanopyrite, Fe-oxyhydroxide) as well as mixed organic phases of Fe as hydrothermal fluids initially mix with oxygenated seawater. High concentrations of weaker ligands have also been observed in samples near the vent orifice in previous studies (Hawkes et al., 2013). These ligands can include humic-like substances, exopolysaccharides, or other organic degradation products (Slagter et al., 2019; Hassler et al., 2020; Mahieu et al., 2024; Hawkes et al., 2013b). In this study, we were not able to discern the exact chemical composition of the ligands we detect via voltammetric methods, and thus the weaker and some portion of the stronger ligands we observe likely represent a mix of different inorganic and organic ligands. Similar to what was described in Hawkes et al. (2013b), the ligands we measure could represent multiple layers of coordination bonds, forming complex Fe phases, similar to the "onion" concept (Mackey and Zirino, 1994). For example, colloidal Fe phases are common in hydrothermal plumes and can form aggregates that bind Fe, but not in traditional organic coordination bonds (Fitzsimmons et al., 2017; Honeyman and Santschi, 1989). There are also likely processes occurring near the vent source in such a complex environment that cause some Fe phases to be in various stages of disequilibria that we also measure as ligands via our voltammetric methods.

The sources of weaker Fe-binding ligands ($\log K^{cond}_{Fe',FeL} < 12$) that have been observed in other hydrothermal plumes is not well understood, and their impact on Fe cycling over the lifetime of neutrally-buoyant plume is unclear. Recent studies have shown microbes may use siderophores or siderophore-like (strong binding ligands) ligands to access Fe associated with weaker ligands — such as humic substances and thiols — to enhance the bioavailability of Fe (Kuhn et al., 2014; Muller, 2018). However, to date, the few studies that have explored ligand concentrations and binding strengths within hydrothermal plumes (Buck et al., 2015; Hawkes et al., 2013c; Buck et al., 2018; Kleint et al., 2016; Sander and Koschinsky, 2011; Mahieu et al., 2024) have mixed hypotheses as to the role and sources of weaker-type ligands within plumes. Additional studies are needed to investigate the sources and mechanisms of weaker-type ligands in hydrothermal plumes and understand their impact on the Fe cycle in hydrothermal plumes.

In the neutrally buoyant plume samples, stronger L_1 ligands were present and were correlated with the dFe concentrations (**Fig. 1**) and weaker ligands were no longer dominant. In other systems with a high dFe and ligand endmember such as estuaries, a decrease in weaker ligands along with dFe concentrations has also been observed (Buck et al., 2007; Bundy et al., 2014). This has been interpreted as a scavenging of weaker Fe-ligand complexes, while the dFe that remains in solution is that which is bound to stronger ligands (Bundy et al., 2014). A similar control on dFe concentrations by L_1 ligands has also been previously observed in aerosol solubility experiments (Fishwick et al., 2014). There are a few possible explanations for the correlation of dFe and L_1 ligands in the neutrally-buoyant plume. One possible explanation is that both the dFe and L_1 ligands originate from the vent fluids themselves, yielding a tightly coupled hydrothermal endmember. However, the concentration of L_1 ligands did not correlate with excess mantle Helium-3 ($^3He_{xs}$, **Fig S2**, **Table S2-S3**) (Lough et al., 2022), a nearly conservative tracer of the mixing of hydrothermal fluids with seawater (Buck et al., 2018). Moreover, our samples closer to the vent source were dominated by weaker organic ligands showing no correlation to dFe. This suggests the L_1 ligands were not directly sourced from the vent fluids along with dFe. Biological sources represent another likely explanation for the coupling of L_1 ligands and dFe, if the ligands observed in the neutrally-buoyant plume are from bacteria that produced them in surrounding deep ocean seawater that was then entrained, local production from vent-biota and/or microbial mats, diffusion from microbial production in sediments, or *in-situ* production by bacteria within the neutrally buoyant plume (Dick et al., 2013; Li et al., 2014; Sheik et al., 2015; Mellett et al., *submitted*.).

2.2 The presence of siderophores in hydrothermal systems

Siderophores were measured in a subset of the samples to further explore the source of the L_1 ligands coupled to dFe in the neutrally-buoyant plume. Marine organic ligand composition changes with environmental gradients (Gledhill and Buck, 2012; Boiteau et al., 2016), making the structure and functional groups of siderophores identified in hydrothermal samples of particular interest. Somewhat surprisingly, siderophores were found in all samples and we observed a large diversity of siderophores with high confidence using mass-to-charge ratio (*m/z*), MS/MS spectra, and specific chromatographic characteristics (**Fig. 2a**). On-axis spreading centers contained the highest dFe concentrations (> 20 nM) and wider variety of siderophores than samples from fracture zones, diffuse, and off-axis sites (dFe ≤ 1 nM). The greatest number of distinct siderophores were identified at Lucky Strike, Broken Spur, Rainbow, and TAG (**Fig. 2**). On average, 13 compounds were identified with high confidence per on-axis spreading center sample, compared with 5 per diffuse/fracture zone sample, and 2.5 per off-axis sample (**Fig. 2b, Fig. S4**). Mixed-type siderophores — containing different moieties that bind to Fe(III) — were common at all sites. Hydroxamates were identified at and around spreading centers, yet none of these were detected with high confidence in samples from diffuse/fracture zones (**Fig. S4**). Summed siderophore abundance in neutrally-buoyant plumes above spreading centers was similarly more than twice that of samples from fracture zones or off-axis (**Fig. 2c**). Thus, vent type and proximity played a role in the diversity and abundance of siderophore types observed, likely related to the diversity of the microbial community and/or unique Fe acquisition strategies across sites.

Siderophores are putatively part of the operational L_1 ligand pool based on their binding strength (Gledhill and Buck, 2012), and patterns in their distributions were similar to those of the strong ligands. The peak areas of each putative siderophore we identified were used as a proxy for concentrations (*section 3.3*), and these concentrations significantly correlated with dFe, as observed with dFe and L_1 ligands (**Fig. 2b**). Siderophores were present in concentrations similar to the surface ocean (Park et al., 2022; Boiteau et al., 2016; Moore et al., 2021; Bundy et al., 2018) and were equivalent to concentrations representing 0.01-0.4% of the total L_1 ligands (**Table 1**). This is a substantial underestimate of siderophore contributions to the L_1 ligand pool due to analytical constraints in identifying unknown siderophores. Recent work on siderophore biosynthesis pathways and advances in genome mining suggest that known siderophores represent a small fraction of what is expected to be produced in nature (Hider and Kong, 2010; Reitz et al., 2022), and our analyses in this study were limited to only known siderophores. We also restricted our reporting to compounds identified with very high confidence (**Fig 2a**, **S3**). In addition, most siderophores are not commercially available to use as standards, and individual siderophores have different ionization or extraction efficiencies. The extraction efficiency for the solid phase extraction technique is approximately 5-10% for bulk Fe-binding organics (Bundy et al., 2018) and 40% for a siderophore standard (Waska et al., 2015). Employing both corrections yields siderophore contributions to the total L_1 pool of 0.1-4% and 0.025-1%, respectively. We are inevitably missing many naturally occurring unknown compounds, and thus we consider this a lower bound. Regardless of the small percentage contribution to total L_1 ligands, it is evident that microbially produced siderophores were ubiquitous across all vent sites and had similar distributional patterns as L_1 ligands. There are also likely other compounds such as some strong binding humics that are also contributing to the L_1 ligand pool (Laglera and van den Berg, 2009). Future work with much larger water volumes will be able to reduce uncertainty and identify a greater number of compounds. Still, the identification of siderophores here — and their relationship with dFe — provides compelling evidence that microbial production of ligands is responsible for at least some portion of the tight coupling between L_1 and dFe in hydrothermal systems along the MAR.

The presence and diversity of siderophores identified in this system was surprising given the relatively high Fe concentrations of hydrothermal environments, but some compelling patterns were observed. Amphiphilic siderophores comprised 57% of the siderophores in our samples (**Fig. S5**), supporting the ubiquity of amphiphilic siderophores in marine environments (Butler and Theisen, 2010). Amphiphilic siderophores were found in concentrations between 0.3-4.7 pM, with the highest concentrations found at Rainbow (**Fig. 2d**, **Table S6**). These concentrations were similar to those observed in the upper ocean (Boiteau et al., 2019, 2016; Bundy et al., 2018). Amphiphilic siderophores have long hydrocarbon tails that can be embedded into the lipid bilayer of the bacterial cell membrane providing a mechanism to shuttle Fe into the cell and prevent diffusive loss (Martinez et al., 2003). Marine bacteria produce suites of amphiphilic siderophores as a way to adapt to the change in hydrophilicity in the surrounding environment (Homann et al., 2009; Sandy and Butler, 2009). Amphiphilic siderophores in plumes could be a way for bacteria to access Fe as they are

physically transported and cope with strong chemical gradients, similar to the production of multiple siderophores in terrestrial and pathogenetic systems as a means to access inorganic particulate Fe for cellular uptake and storage (Hider and Kong, 2010).

2.3 Microbial sources of siderophores in hydrothermal plumes

The high diversity of siderophores across a huge range of hydrothermal vent systems revealed several surprising aspects of Fe cycling. The biosynthesis of a siderophore is energy-intensive and is regulated by Fe concentration in the surrounding environment (Rizzi et al., 2019). Siderophore presence suggests that bacteria are producing these compounds despite the overall higher Fe concentrations in the deep ocean and within hydrothermal plumes. Consistent with siderophore utilization in terrestrial ecosystems (Hider and Kong, 2010; Sandy and Butler, 2009), one hypothesis is that siderophore production is beneficial to bacteria in the plumes for transforming Fe from otherwise inaccessible forms, such as particulate nanopyrites or Fe oxyhydroxides that are present close to the vent source. To explore the potential for microbial production of siderophores, we examined microbial community composition around Rainbow (St. 11, 17) and Lucky Strike (St. 7; **Table 1, Table S1**) using 16S rRNA gene-based amplicon sequencing to detect bacteria with the metabolic potential to synthesize siderophores (**Fig. 3, S11**). The presence of taxa encoding siderophore biosynthetic gene clusters indicates whether the microbial community has the genetic potential of producing the compounds we observed. Bacterial genera containing known siderophore-producers were found at all three MAR sites examined, and putative siderophore-producers represented 3-20% of the relative abundance of the community (**Fig. 3**). Putative siderophore-producers were more abundant in the 3 μm (particle-attached) size fraction than in the 0.2 μm (free-living) fraction, suggesting siderophore production is more common in particle-associated bacteria in hydrothermal environments.

We found microbial genera in our samples that can produce a subset of the siderophores identified here, including ferrioxamines, vibrioferrin, and acinetoferrin (Vraspir and Butler, 2009; Butler, 2005; Moore et al., 2021; Bundy et al., 2018; Boiteau et al., 2016). Genera with the genetic potential to produce ferrioxamines were present at all three sites, while those known to produce vibrioferrin were present at Lucky Strike and Rainbow, and those producing acinetoferrin were also present at Rainbow (**Table S1, S7**). Mycobactins were detected with high confidence in every sample of this study, and genes encoding mycobactin have been detected in a cultured organism from a hydrothermal system (Gu et al., 2019), but no mycobactin producers were identified in this study. We detected woodybactin D with high confidence in 5 out of 11 sites analysed and compared to the known siderophore library (**Fig. 2**). Woodybactin D biosynthetic genes were not identified in any of the genera from the 16S rRNA gene amplicon sequences.; however, woodybactin D is a carboxylate siderophore isolated from *Shewanella* (Carmichael et al., 2019), and groups of deep-sea *Shewanella* (Kato and Nogi, 2001) were found in the dataset (**Fig. S11**). The biosynthesis genes for many of the siderophores identified are unknown. Thus, finding genera capable of producing only a subset of the

siderophores characterized is not surprising. The observation that a portion of the *in-situ* microbial community is capable of synthesizing siderophores (**Fig. 3**) suggests that siderophore production is more widespread in the deep ocean than previously believed and could contribute to the "microbial iron pump" in hydrothermal plumes (Li et al., 2014)

2.4 The impact of strong ligands and siderophores on dissolved iron in neutrally-buoyant plumes

Evidence that siderophores are ubiquitous in the marine environment — including higher Fe environments — has been increasing (Park et al., 2022). The high dFe associated with hydrothermal plumes may still not be high enough to suppress siderophore production due to the elevated Fe requirements of heterotrophic bacteria (Tortell et al., 1996). It is also likely that not all of the Fe is bio-accessible in hydrothermal plumes. Soil microbes secrete siderophores to solubilize particulate Fe (Crowley et al., 1991) and similar processes could be occurring in hydrothermal plumes, where Fe mineral phases associated with organic compounds are common (Hoffman et al., 2020; Toner et al., 2009; Hoffman et al., 2018; German and Seyfried, 2014; Holden et al., 2012; Fitzsimmons et al., 2017). Although our measurements suggest that dFe in the neutrally-buoyant plume is likely dominated by organic complexation, the L_1 measurements alone cannot distinguish between purely organic phases or a mixture of inorganic and organic ligands in complex aggregations or small colloids, as discussed above (*section 2.1*). Given the evidence from particulate Fe studies in neutrally-buoyant plumes (Yücel et al., 2011; Fitzsimmons et al., 2014; Hoffman et al., 2020; Toner et al., 2009; Fitzsimmons et al., 2017; Hoffman et al., 2018), it is highly likely that some portion of what is detected in the L_1 pool is a mixture of organic and inorganic Fe in small colloids which are operationally in the dFe pool (Fitzsimmons et al., 2017). It is also telling that 4-5x more siderophore-producing genera were found to be particle-associated (**Fig. 3**), providing additional evidence that siderophores might be produced to solubilize particulate Fe or access other colloidal phases. Further work that assesses why bacteria are producing siderophores in neutrally buoyant plumes will be important for understanding microbial metabolism in these systems, and the impact of siderophore production on Fe dispersal.

Organic Fe-binding ligands have been implicated in playing a critical role in the preservation and transport of hydrothermal dFe into the ocean interior (Bennett et al., 2011; Hoffman et al., 2018; Fitzsimmons et al., 2017; Toner et al., 2009; Bennett et al., 2008; Resing et al., 2015; Buck et al., 2018; Sander and Koschinsky, 2011). In this work, L_1 ligands were tightly coupled to dFe in neutrally buoyant plumes along the MAR and the presence of siderophores in these samples provided evidence for the first time, that at least some of these ligands are microbially produced. How these complexes may facilitate the exchange of Fe between dissolved and particulate phases (Fitzsimmons et al., 2017), and whether siderophores are present across additional hydrothermal vent systems will aid in understanding how microorganisms might play a role in shaping the hydrothermal dFe supply to the deep ocean.

3. Appendix: Materials and Methods

3.1 Sampling and cruise transect

Samples were collected as part of the 2017-2018 U.K. GEOTRACES GA13 section cruise along the Mid-Atlantic Ridge (FRidge GA13). Water samples from 11 venting and near venting locations were collected using a Seabird 911 conductivity, temperature, and depth (CTD) titanium rosette using conducting Kevlar wire with an oxidation-reduction potential (ORP) sensor to detect plumes. Teflon coated OTE (Ocean Test Equipment) bottles were pressurized to approximately 7 psi with 0.2 µm filtered air using an oil free compressor. A Sartobran 300 (Sartorius) filter capsule (0.2 µm) was used to collect filtered seawater samples into clean 250 mL LDPE sample bottles. Bottles and caps were rinsed 3 times with the filtered sample before being filled. Samples were stored frozen at -20˚C for Fe-organic ligand characterization by voltammetry and mass spectrometry.

3.2 Fe-binding ligand concentration and binding strengths Competitive Ligand Exchange-Adsorptive Cathodic Stripping Voltammetry

Fe-binding ligand concentrations and binding strengths (defined as conditional binding constants, log $K^{cond}_{Fe',FeL}$ > 12) were determined by competitive ligand exchange-adsorptive cathodic stripping voltammetry (CLE-ACSV) with a BAS*i* controlled growth mercury electrode (CGME) with an Ag/AgCl^{-} reference electrode and platinum auxiliary electrode (Bioanalytical Systems Incorporated). Using previously established methods (Abualhaija and van den Berg, 2014; Buck et al., 2015; Hawkes et al., 2013c; Buck et al., 2018; Bundy et al., 2018), 40 frozen filtrate (<0.2 µm) samples with dFe concentrations between 0.41-11.67 nM (**Table S1-S2**) were thawed in a 4˚C fridge prior to analysis. A 15-point titration curve was analyzed for each sample. Briefly, within each titration, every point sequentially received 10 mL of sample, 7.5 mM of borate-ammonium buffer, 10 µM salicylaldoxime (SA) added ligand, and a dFe addition (see Supplemental Methods 1.1. for additional details). Samples were then equilibrated overnight before being measured on the BAS*i*. Data was collected using the *Epsilon Eclipse Electrochemical Analyzer* (v.213) with a deposition time of 120 seconds and analyzed using *ElectroChemical Data Software* (v2001-2014) and *ProMCC* (v2008-2018) to determine peak areas and Fe-binding ligand parameters, respectively. All results were confirmed to fall within the analytical window of the method by comparing the side reaction coefficient of the added ligand α_{SA} to the side reaction coefficient of the natural ligands detected (α_L). If the α_L was within an order of magnitude of α_{SA} then the results were deemed to fall within the analytical window.

3.3 Reverse Titration-CLE-ACSV

Reverse titration-CLE-ACSV (RT-CLE-ACSV) (Hawkes et al., 2013a) was completed on 10 samples from Broken Spur, and TAG hydrothermal vent fields with dFe concentrations between 19.01-90.25 nM (**Table S3**). Briefly, a 10-point titration curve was analyzed for each sample with each titration point consisting of 10 mL of sample buffered with 7.5 mM boric acid and the competitive ligand 1-nitroso-2-napthol (NN) additions. All samples were analyzed on a BAS*i* Controlled Growth Mercury Electrode (CGME) with the

Epsilon Eclipse Electrochemical Analyzer (v.213) and deposition time of 120 seconds. For each sample, competitive ligand NN additions were 0.5, 1, 2, 3, 4, 6, 9, 15, 20, and 40 µM. Samples were equilibrated overnight and purged with N_2 (99.99%) for 5 minutes before analysis. At the end of each titration, three Fe additions (3-15 nM) were added to the final titration point to get the total concentration of Fe in equilibrium with ligands. Data was analyzed using *ElectroChemical Data Software* (v2001-2014) to acquire peak areas and a package in R using the model parameters of $\beta_{FeNN3} = 5.12 \times 10^{16}$, $\chi_{min} = 0.8$, $\chi_{max} = 0.9$, and $c1high = 0.75$ to determine the Fe-binding ligand parameters (Hawkes et al., 2013a). These parameters were chosen based on the recommendations for undersaturated samples and titrations curves where ip_{max} was not reached (Hawkes et al., 2013a). All other parameters within the model we kept at the default values.

3.4 Siderophore quantification and characterization

In addition to measuring Fe-binding ligands by voltammetry, we also identified and quantified siderophores. Between 0.65-1.5 L of 0.2 µm filtered seawater pooled from ligand samples at each site (described above) was pumped slowly (15-20 mL min^{-1}) onto a polystyrene-divinylbenzene (Bond Elut ENV) solid phase extraction (SPE) column (Bundy et al., 2018; Boiteau et al., 2016). SPE columns were rinsed with MilliQ and stored at -20ºC until analysis. For the analytical measurements, samples were thawed in the dark, eluted in 12 mL of distilled methanol, and dried down to between 0.2-0.5 mL of sample eluent (**Table S1**). Aliquots were analyzed by reverse-phase liquid chromatography (LC) on a trace metal clean bio-inert LC (Thermo Dionex 3000 NCS). The LC was interfaced with an electrospray ionization-mass spectrometer (ESI-MS; Thermo Q-Exactive HF) to identify and quantify the compounds based on accurate mass (MS^1) and the fragmentation (MS^2) data (Bundy et al., 2018; Boiteau et al., 2016). MSconvert (Proteowizard) was used to convert MS data to an open source mzxML format, and two stages of data processing were conducted using modified versions of previously reported R scripts (Bundy et al., 2018; Boiteau et al., 2016). In the first stage, mzxML files were read into R using new package "RaMS" (Kumler and Ingalls, 2022) , and extracted ion chromatograms (EICs) were generated for each targeted *m/z* of interest from an in-house database of siderophores. The *m/z* targets were the ionized apo, ^{54}Fe-bound, and ^{56}Fe-bound version of each siderophore, with a tolerance of 7.5 ppm. Putative siderophore candidates were filtered through a series of hard thresholds, such that MS^1 spectra were quality controlled to contain a minimum of 25 datapoints and the maximum intensity of each EIC was greater than 1e4 counts. Spectra meeting these criteria and containing either ^{54}Fe-bound and ^{56}Fe-bound *m/z* peaks within 30 seconds of each other or an apo peak were displayed for the user to further inspect peak quality and make the final decision of whether to move on to stage two of processing with a given siderophore candidate.

Stage two of processing extracted MS^2 spectra of the apo and Fe-bound forms of candidate siderophores to compare with the predicted MS^2 generated by *in silico* fragmenter MetFrag (Ruttkies et al., 2016). The *in silico* fragmenter feature was run with a tolerance of 10 ppm on "$[M+H]^+$" and "$[M+Na]^+$" modes. A confidence level of 1-4, from highest to lowest confidence, was then assigned to putative siderophores based

on the following criteria: (1) peaks were present in MS^1 and MS^2 spectra, and at least one of the three most-intense MS^2 fragments matched *in silico* fragmentation, (2) peaks were present in MS^1 and MS^2 spectra, and smaller-intensity fragments matched *in silico* fragmentation, (3) peaks were present in MS^1 and MS^2 spectra, but little to no fragments matched *in silico* fragmentation, and (4) nicely shaped peaks were identified in MS^1 spectra but no MS^2 spectra was collected (outlined in **Table S5**; example spectra in **Fig. S6-S9)**. The confidence levels were modelled after reporting standards for metabolite identification (Sumner et al., 2007). MetFrag pulls chemical structures from publicly-available databases like PubChem or COCONUT (Sorokina et al., 2021), which contain most, but not all variations of siderophores. As such, Fe-bound candidates were usually run against the apo form available in the database, and for siderophores with similar structures but variations in fatty chain length or double bond placement, sometimes only one parent structure was available.

A 5-point standard curve with known concentrations of siderophore ferrioxamine E was used for quantification of putative siderophores, with a limit of detection of 0.257 nM in the eluent (**Fig. S10**), or 0.07-0.21 pM in the sample depending on sample-to-eluent volume ratio at each site (**Table S1**). MS^1 peaks were integrated for all putatively identified siderophores and peak areas were converted to concentration using the standard curve and the concentration factor of sample volume to eluent volume (**Fig. S10**). Commercial standards are not available for most siderophores, and different compounds have distinct ionization efficiencies in ESI-MS. Thus, the siderophore concentrations reported here are estimates of siderophore concentrations in these environments based on ferrioxamine E, chosen for its commercial availability and use in prior studies (e.g., (Boiteau et al., 2016)). Additionally, 1 mM of cyanocobalamin was added as an internal standard to each sample aliquot to address any changes in sensitivity during LC-ESI-MS runs. All putative siderophores that were identified with peak areas less than the detection limit were discarded, and all remaining putative compounds with at least confidence levels 1 and 2 at one site were included in the manuscript and are referred to as siderophores throughout. Siderophore identifications remain putative due to inherent uncertainty with assignments by mass, but the confidence levels were designed such that high confidence candidates contain siderophore-like moieties in their fragments. Limited sample volumes prevented analysis via LC-ICP-MS like previous studies, which, in addition to greater availability of commercial standards and more analytical comparisons between ferrioxamine E with other siderophore types, would allow definitive characterization in future studies. Confidence level 3 and 4 putative siderophores are only included in the Supplementary Information (**Table S6**). In a final step of quality control, EICs for ^{13}C isotopologues of candidates were inspected to verify matching peak structure.

3.5 Microbial community analysis

Microbial community composition was assessed in neutrally buoyant plumes and near venting sites at three sites: Lucky Strike (Station 7; 1670 m), 10 km S of Rainbow (Station 17; 2000 m), and 200 km E of Rainbow (Station 11; 600 m, 1600 m and 2250 m). A range of 1- 2 L of seawater were filtered by pressure filtration through sequential 25 mm membrane filters housed in polypropylene filter holders (Whatman SwinLok, GE

Healthcare, Pittsburgh, Pennsylvania) using a peristaltic pump and silicone tubing. Samples first passed through a 3 μm pore-size polyester membrane filter (Sterlitech, Auburn, Washington) then onto a 0.2 μm pore-size polyethersulfone membrane filter (Supor-200, Pall Corporation, Port Washington, New York). Pump tubing was acid washed with 10% hydrochloric acid and flushed with ultrapure water between each sample. The filters were flash frozen in liquid nitrogen in 2 mL gasketed bead beating tubes (Fisher Scientific) at sea.

Nucleic acids (DNA) were extracted as described previously (Santoro et al., 2010), with slight modifications. Briefly, cells on the filters were lysed directly in the bead beating tubes with sucrose-ethylene diamine tetraacetic acid (EDTA) lysis buffer (0.75 M sucrose, 20 mM EDTA, 400 mM NaCl, 50 mM Tris) and 1% sodium dodecyl sulfate. Tubes were then agitated in a bead beating machine (Biospec Products) for 1 min, and subsequently heated for 2 min. at 99°C in a heat block. Proteinase K (New England Biolabs) was added to a final concentration of 0.5 mg/mL. Filters were incubated at 55°C for approximately 4 h and the resulting lysates were purified with the DNeasy kit (Qiagen) using a slightly modified protocol (Santoro et al., 2010). The purified nucleic acids were eluted in 200 μL of DNase, RNase-free water, and quantified using a fluorometer (Qubit and Quanti-T HS reagent, Invitrogen Molecular Probes).

The 16S rRNA gene was amplified in all samples using V4 primers (Apprill et al., 2015; Parada et al., 2016) (515F-Y and 806RB) following a previously established protocol (Stephens et al., 2020). Amplicons were sequenced using a paired-end 250bp run on an Illumina MiSeq 500 and demultiplexed by the UC Davis Genome Center. The resulting 16S rRNA amplicon sequences were filtered and trimmed using the DADA2 pipeline in R(Callahan et al., 2016). Taxonomic assignments were made with version 138.1 of the SILVA SSU database (Quast et al., 2013) (silva_nr99_v138.1_wSpecies_train_set.fa.gz ; doi:10.5281/zenodo.4587955; accessed March 2022). Chloroplast and mitochondrial sequences were filtered out of the dataset using the 'phyloseq' R package (v 1.38.0), after which samples had read depths ranging from 9375 – 65486 reads (average 28425 $\pm$ 20014 reads) and represented 1010 unique amplicon sequence variants (ASVs). Read counts were transformed from absolute to relative abundance and taxa were aggregated to the Family level. The ten most abundant families present in each sample were visualized using the 'ggplot2' package (v. 3.3.5).

In order to assess the potential of the observed prokaryotic taxa to produce siderophores, we downloaded all siderophore biosynthetic gene clusters (BGCs) in the v3 antiSMASH secondary metabolite database (n = 7909) and used text-string matching to compare genera containing these BGCs to the genera found in our 16S rRNA gene dataset (Blin et al., 2021). We cross-referenced the nomenclature of antiSMASH-predicted siderophores with that of the siderophores identified by LC-ESI-MS in this study, accounting for minor differences in naming convention between the two databases, to determine if microbial community members present at each site were predicted to make any of the siderophores that were measured at that site. Station

38 and Station 12 were the closest sites with siderophore measurements for comparison against the taxonomic samples taken at 200 km E of Rainbow and 10 km S of Rainbow, respectively. Samples for microbial taxonomy and siderophore identity were taken from the same location at Lucky Strike and thus directly compared.

Data Availability

The CSV data reported in this study has been deposited at Zenodo under the DOI: http://doi.org/10.5281/zenodo.7325154. The LC-ES-MS data has been deposited on Massive under the DOI: http://doi.org/doi.10.25345/C5V97ZW7N. Microbial 16S rRNA data have been deposited on GenBank under the accession number BioProject #PRJNA865382. All data is freely available on each of these data repositories.

Acknowledgments

We acknowledge the captain and crew of the R/V *James Cook*, Chief Scientist Alessandro Tagliabue, and Noah Gluschankoff for supporting this work. This study was a part of the FeRidge project (GEOTRACES section GA13) which was supported by the Natural Environment Research Council funding (NERC United Kingdom Grants NE/N010396/1 to MCL and NE/N009525/1 to AT). The International GEOTRACES Programme is possible in part thanks to the support from the U.S. National Science Foundation (Grant OCE-1840868) to the Scientific Committee on Oceanic Research (SCOR). CLH was funded by JISAO/CICOES postdoctoral fellowship. PJM was funded through the NOAA Hollings Scholar summer program. JR was funded by NOAA Ocean Exploration and Research, NOAA Earth-Ocean Interactions programs at NOAA-Pacific Marine Environmental Lab (PMEL #5955), and UW-CICOES (CICOES #2024-1385). Part of this work was carried out in the University of Washington TraceLab, which receives support from the M.J. Murdock Charitable Trust in conjunction with the University of Washington College of Environment, and the Pacific Marine Environmental Labs at the National Oceanic and Atmospheric Administration. Parts of this work was also carried out in Dr. Anitra Ingalls laboratory with the help of Laura Truxal and Dr. Jiwoon Park at the University of Washington-School of Oceanography.

Author Contributions: Manuscript preparation, sample/data processing, CSV analysis, and interpretation LC-ESI-MS data analysis and interpretation (C.L.H. and P.J.M.), microbial analysis and interpretation (J.B.A. and A.E.S.), dissolved iron and derived excess $^{3}He_{xs}$ measurements, sample collection (A.J.M. L. and M.C.L.), microbial data collection and ligand data interpretation (T.M. and K.N.B.), and project design and planning, data interpretation, and mentoring (A.T., M.C.L., J.A.R., and R.M.B.). All authors were involved in editing and revision of the manuscript.

Competing Interest Statement: The authors declare no competing interests.

References

Abualhaija, M. M. and van den Berg, C. M. G.: Chemical speciation of iron in seawater using catalytic cathodic stripping voltammetry with ligand competition against salicylaldoxime, Mar. Chem., 164, 60–74, https://doi.org/10.1016/j.marchem.2014.06.005, 2014.

Aguilar-Islas, A. M., Wu, J., Rember, R., Johansen, A. M., and Shank, L. M.: Dissolution of aerosol-derived iron in seawater: Leach solution chemistry, aerosol type, and colloidal iron fraction, Mar. Chem., 120, 25–33, 2010.

Apprill, A., Mcnally, S., Parsons, R., and Weber, L.: Minor revision to V4 region SSU rRNA 806R gene primer greatly increases detection of SAR11 bacterioplankton, Aquat. Microb. Ecol., 75, 129–137, https://doi.org/10.3354/ame01753, 2015.

Bazylev, B. A.: Allochemical Metamorphism of Mantle Peridoties in the Hayes Fracture Zone of the North Atlantic, Petrology, 5, 362–379, 1997.

Beaulieu, S. E. and Szafrański, K. M.: InterRidge Global Database of Active Submarine Hydrothermal Vent Fields Version 3.4, https://doi.org/10.1594/PANGAEA.917894, 2020.

Bennett, S. a., Achterberg, E. P., Connelly, D. P., Statham, P. J., Fones, G. R., and German, C. R.: The distribution and stabilisation of dissolved Fe in deep-sea hydrothermal plumes, Earth Planet. Sci. Lett., 270, 157–167, https://doi.org/10.1016/j.epsl.2008.01.048, 2008.

Bennett, S. a., Hansman, R. L., Sessions, A. L., Nakamura, K. ichi, and Edwards, K. J.: Tracing iron-fueled microbial carbon production within the hydrothermal plume at the Loihi seamount, Geochim. Cosmochim. Acta, 75, 5526–5539, https://doi.org/10.1016/j.gca.2011.06.039, 2011.

Blin, K., Shaw, S., Kautsar, S. A., Medema, M. H., and Weber, T.: The antiSMASH database version 3: Increased taxonomic coverage and new query features for modular enzymes, Nucleic Acids Res., 49, D639–D643, https://doi.org/10.1093/nar/gkaa978, 2021.

Boiteau, R. M., Mende, D. R., Hawco, N. J., McIlvin, M. R., Fitzsimmons, J. N., Saito, M. A., Sedwick, P. N., DeLong, E. F., and Repeta, D. J.: Siderophore-based microbial adaptations to iron scarcity across the eastern Pacific Ocean, Proc. Natl. Acad. Sci., 113, 14237–14242, https://doi.org/10.1073/pnas.1608594113, 2016.

Boiteau, R. M., Till, C. P., Coale, T. H., Fitzsimmons, J. N., Bruland, K. W., and Repeta, D. J.: Patterns of iron and siderophore distributions across the California Current System, Limnol. Oceanogr., 64, 376–389, https://doi.org/10.1002/lno.11046, 2019.

Buck, K. N., Sohst, B., and Sedwick, P. N.: The organic complexation of dissolved iron along the U.S. GEOTRACES (GA03) North Atlantic Section, Deep. Res. Part II Top. Stud. Oceanogr., 116, 152–165, https://doi.org/10.1016/j.dsr2.2014.11.016, 2015.

Buck, K. N., Sedwick, P. N., Sohst, B., and Carlson, C. A.: Organic complexation of iron in the eastern tropical South Pacific: Results from US GEOTRACES Eastern Pacific Zonal Transect (GEOTRACES cruise GP16), Mar. Chem., 201, 229–241, https://doi.org/10.1016/j.marchem.2017.11.007, 2018.

Bundy, R. M., Boiteau, R. M., McLean, C., Turk-Kubo, K. A., McIlvin, M. R., Saito, M. A., Mooy, B. A. Van, and Repeta, D. J.: Distinct Siderophores Contribute to Iron Cycling in the Mesopelagic at Station ALOHA, Front. Mar. Sci., 1–15, https://doi.org/10.3389/fmars.2018.00061, 2018.

Butler, A.: Marine siderophores and microbial iron mobilization., Biometals, 18, 369–374,

https://doi.org/10.1007/s10534-005-3711-0, 2005.

Butler, A. and Theisen, R. M.: Iron(III)-siderophore coordination chemistry: Reactivity of marine siderophores., Coord. Chem. Rev., 254, 288–296, https://doi.org/10.1016/j.ccr.2009.09.010, 2010.

Callahan, B. J., McMurdie, P. J., Rosen, M. J., Han, A. W., Johnson, A. J. A., and Holmes, S. P.: DADA2: High-resolution sample inference from Illumina amplicon data, Nat. Methods, 13, 581–583, https://doi.org/10.1038/nmeth.3869, 2016.

Carmichael, J. R., Zhou, H., and Butler, A.: A suite of asymmetric citrate siderophores isolated from a marine Shewanella species, J. Inorg. Biochem., 198, 1–6, https://doi.org/10.1016/j.jinorgbio.2019.110736, 2019.

Cowen, J. P. and Bruland, K. W.: Metal deposits associated with bacteria: implications for Fe and Mn marine biogeochemistry, Deep Sea Res. Part A. Oceanogr. Res. Pap., 32, 253–272, https://doi.org/10.1016/0198-0149(85)90078-0, 1985.

Cowen, J. P., Massoth, G. J., and Feely, R. A.: Scavenging rates of dissolved manganese in a hydrothermal vent plume, Deep Sea Res. Part A. Oceanogr. Res. Pap., 37, 1619–1637, https://doi.org/10.1016/0198-0149(90)90065-4, 1990.

Crowley, D. E., Wang, Y. C., Reid, C. P. P., and Szaniszlo, P. J.: Mechanisms of iron acquisition from siderophores by microorganisms and plants, Plant Soil, 130, 179–198, 1991.

Dick, G. J., Anantharaman, K., Baker, B. J., Li, M., Reed, D. C., and Sheik, C. S.: The microbiology of deep-sea hydrothermal vent plumes: Ecological and biogeographic linkages to seafloor and water column habitats, Front. Microbiol., 4, 1–16, https://doi.org/10.3389/fmicb.2013.00124, 2013.

Fishwick, M. P., Sedwick, P. N., Lohan, M. C., Worsfold, P. J., Buck, K. N., Church, T. M., and Ussher, S. J.: The impact of changing surface ocean conditions on the dissolution of aerosol iron, Global Biogeochem. Cycles, 28, 1235–1250, https://doi.org/10.1002/2014GB004921, 2014.

Fitzsimmons, J. N. and Boyle, E. A.: Assessment and comparison of Anopore and cross flow filtration methods for the determination of dissolved iron size fractionation into soluble and colloidal phases in seawater, Limnol. Oceanogr. Methods, 12, 246–263, https://doi.org/10.4319/lom.2014.12.246, 2014.

Fitzsimmons, J. N., Boyle, E. a., and Jenkins, W. J.: Distal transport of dissolved hydrothermal iron in the deep South Pacific Ocean, Proc. Natl. Acad. Sci., 111, 16654–16661, https://doi.org/10.1073/pnas.1418778111, 2014.

Fitzsimmons, J. N., John, S. G., Marsay, C. M., Hoffman, C. L., Nicholas, S. L., Toner, B. M., German, C. R., and Sherrell, R. M.: Iron persistence in the distal hydrothermal plume supported by dissolved – particulate exchange, Nat. Geosci., 10, 1–8, https://doi.org/10.1038/ngeo2900, 2017.

German, C. and Seyfried, W. E.: Hydrothermal Processes, 2nd ed., Elsevier Ltd., 1–39 pp., https://doi.org/10.1016/B978-0-08-095975-7.00201-1, 2014.

Gledhill, M. and Buck, K. N.: The organic complexation of iron in the marine environment: A review, Front. Microbiol., 3, 1–17, https://doi.org/10.3389/fmicb.2012.00069, 2012.

Gu, H., Sun, Q., Luo, J., Zhang, J., and Sun, L.: A First Study of the Virulence Potential of a Bacillus subtilis Isolate From Deep-Sea Hydrothermal Vent, Front. Cell. Infect. Microbiol., 9, 1–14, https://doi.org/10.3389/fcimb.2019.00183, 2019.

Hassler, C., Cabanes, D., Blanco-ameijeiras, S., Sander, S. G., and Benner, R.: Importance of refractory ligands and their photodegradation for iron oceanic inventories and cycling, Mar. Freshw. Res., 71, 311–320, 2020.

Hassler, C. S., van den Berg, C. M. G., and Boyd, P. W.: Toward a regional classification to provide a more

inclusive examination of the ocean biogeochemistry of iron-binding ligands, Front. Mar. Sci., 4, https://doi.org/10.3389/fmars.2017.00019, 2017.

Hawkes, J. A., Gledhill, M., Connelly, D. P., and Achterberg, E. P.: Characterisation of iron binding ligands in seawater by reverse titration, Anal. Chim. Acta, 766, 53–60, https://doi.org/10.1016/j.aca.2012.12.048, 2013a.

Hawkes, J. A., Connelly, D. P., Gledhill, M., and Achterberg, E. P.: The stabilisation and transportation of dissolved iron from high temperature hydrothermal vent systems, Earth Planet. Sci. Lett., 375, 280–290, https://doi.org/10.1016/j.epsl.2013.05.047, 2013b.

Hawkes, J. A., Connelly, D. P., Gledhill, M., and Achterberg, E. P.: The stabilisation and transportation of dissolved iron from high temperature hydrothermal vent systems, Earth Planet. Sci. Lett., 375, 280–290, https://doi.org/10.1016/j.epsl.2013.05.047, 2013c.

Hider, R. C. and Kong, X.: Chemistry and biology of siderophores, Nat. Prod. Rep., 27, 637–657, https://doi.org/10.1039/b906679a, 2010.

Hoffman, C. L., Nicholas, S. L., Ohnemus, D. C., Fitzsimmons, J. N., Sherrell, R. M., German, C. R., Heller, M. I., Lee, J. mi, Lam, P. J., and Toner, B. M.: Near-field iron and carbon chemistry of non-buoyant hydrothermal plume particles, Southern East Pacific Rise 15°S, Mar. Chem., 201, 183–197, https://doi.org/10.1016/j.marchem.2018.01.011, 2018.

Hoffman, C. L., Schladweiler, C., Seaton, N. C. A., Nicholas, S. L., Fitzsimmons, J., Sherrell, R. M., German, C. R., Lam, P., and Toner, B. M.: Diagnostic morphology and solid-state chemical speciation of hydrothermally derived particulate Fe in a long-range dispersing plume, ACS Earth Sp. Chem., 4, 1831–1842, https://doi.org/10.1021/acsearthspacechem.0c00067, 2020.

Holden, J., Breier, J., Rogers, K., Schulte, M., and Toner, B.: Biogeochemical processes at hydrothermal vents: microbes and minerals, bioenergetics, and carbon fluxes, Oceanography, 25, 196–208, https://doi.org/http://dx.doi.org/10.5670/oceanog.2012.18, 2012.

Homann, V. V, Sandy, M., Tincu, J. A., Templeton, A. S., Tebo, B. M., and Butler, A.: Loihichelins A - F , a Suite of Amphiphilic Siderophores Produced by the Marine Bacterium Halomonas LOB-5, J. Nat. Prod., 72, 884–888, 2009.

Honeyman, B. D. and Santschi, P. H.: A Brownian-pumping model for oceanic trace metal scavenging: evidence from Th isotopes, 1989.

Kato, C. and Nogi, Y.: Correlation between phylogenetic structure and function : examples from deep-sea Shewanella, 35, 223–230, 2001.

Kelley, D. S. and Shank, T. M.: Hydrothermal systems: A decade of discovery in slow spreading environments, Geophys. Monogr. Ser., 188, 369–407, https://doi.org/10.1029/2010GM000945, 2010.

Kleint, C., Hawkes, J. A., Sander, S. G., and Koschinsky, A.: Voltammetric Investigation of Hydrothermal Iron Speciation, Front. Mar. Sci., 3, 1–11, https://doi.org/10.3389/fmars.2016.00075, 2016.

Kuhn, K. M., Maurice, P. A., States, U., Neubauer, E., Hofmann, T., and Kammer, F. Von Der: Accessibility of Humic-Associated Fe to a Microbial Siderophore: Implications for Bioavailability, Environ. Sci. Technol., 1015–1022, 2014.

Kumler, W. and Ingalls, A. E.: The R Journal: Tidy Data Neatly Resolves Mass-Spectrometry's Ragged Arrays, R J., 2022.

Laglera, L. M. and van den Berg, C. M. G.: Evidence for geochemical control of iron by humic substances in seawater, Limnol. Oceanogr., 54, 610–619, 2009.

592 Lauderdale, J. M., Braakman, R., Forget, G., Dutkiewicz, S., and Follows, M. J.: Microbial feedbacks
593 optimize ocean iron availability, Proc. Natl. Acad. Sci. U. S. A., 117, 4842–4849,
594 https://doi.org/10.1073/pnas.1917277117, 2020.

595 Li, M., Toner, B. M., Baker, B. J., Breier, J. a, Sheik, C. S., and Dick, G. J.: Microbial iron uptake as a
596 mechanism for dispersing iron from deep-sea hydrothermal vents., Nat. Commun., 5, 3192,
597 https://doi.org/10.1038/ncomms4192, 2014.

598 Lough, A. J. M., Homoky, W. B., Connelly, D. P., Nakamura, K., Abyaneh, M. K., Kaulich, B., and Mills,
599 R. A.: Soluble iron conservation and colloidal iron dynamics in a hydrothermal plume, Chem. Geol.,
600 https://doi.org/10.1016/j.chemgeo.2019.01.001, 2019.

601 Lough, A. J. M., Tagliabue, A., Demasy, C., Resing, J. A., Mellett, T., Wyatt, N. J., and Lohan, M. C.: The
602 impact of hydrothermal vent geochemistry on the addition of iron to the deep ocean, Biogeosciences Discuss.,
603 [preprint], 1–23, https://doi.org/10.5194/bg-2022-73, 2022.

604 Mackey, D. J. and Zirino, A.: Comments on trace metal speciation in seawater or do “onions” grow in the
605 sea?, Anal. Chim. Acta, 284, 635–647, 1994.

606 Mahieu, L., Whitby, H., Dulaquais, G., Tilliette, C., Guigue, C., Tedetti, M., Lefevre, D., Fourrier, P.,
607 Bressac, M., Sarthou, G., Bonnet, S., Guieu, C., and Salaün, P.: Iron-binding by dissolved organic matter in
608 the Western Tropical South Pacific Ocean (GEOTRACES TONGA cruise GPpr14), Front. Mar. Sci., 11,
609 https://doi.org/10.3389/fmars.2024.1304118, 2024.

610 Manck, L. E., Park, J., Tully, B. J., Poire, A. M., Bundy, R. M., Dupont, C. L., and Barbeau, K. A.:
611 Petrobactin, a siderophore produced by Alteromonas, mediates community iron acquisition in the global
612 ocean, ISME J., 16, 358–369, https://doi.org/10.1038/s41396-021-01065-y, 2022.

613 Martinez, J. S., Carter-Franklin, J. N., Mann, E. L., Martin, J. D., Haygood, M. G., and Butler, A.: Structure
614 and membrane affinity of a suite of amphiphilic siderophores produced by a marine bacterium, Proc. Natl.
615 Acad. Sci. U. S. A., 100, 3754–3759, https://doi.org/10.1073/pnas.0637444100, 2003.

616 Mellett, T., Albers, J. B., Santoro, A., Wang, W., Salaun, P., Resing, J., Lough, A. J. ., Tagliabue, A., Lohan,
617 M., Bundy, R. M., and Buck, K. N.: Particle exchange mediated by organic ligands in incubation experiments
618 of hydrothermal vent plumes along the mid-Atlantic Ridge, n.d.

619 Misumi, K., Lindsay, K., Moore, J. K., Doney, S. C., Tsumune, D., and Yoshida, Y.: Humic substances may
620 control dissolved iron distributions in the global ocean: Implications from numerical simulations, Global
621 Biogeochem. Cycles, 27, 450–462, 2013.

622 Moore, L. E., Heller, M. I., Barbeau, K. A., Moffett, J. W., and Bundy, R. M.: Organic complexation of iron
623 by strong ligands and siderophores in the eastern tropical North Pacific oxygen deficient zone, Mar. Chem.,
624 236, 104021, https://doi.org/10.1016/j.marchem.2021.104021, 2021.

625 Muller, F. L. L.: Exploring the Potential Role of Terrestrially Derived Humic Substances in the Marine
626 Biogeochemistry of Iron, Front. Earth Sci., 6, 1–20, https://doi.org/10.3389/feart.2018.00159, 2018.

627 Omanović, D., Garnier, C., and Pižeta, I.: ProMCC: An all-in-one tool for trace metal complexation studies,
628 Mar. Chem., 173, 25–39, https://doi.org/10.1016/j.marchem.2014.10.011, 2015.

629 Parada, A. E., Needham, D. M., and Fuhrman, J. A.: Every base matters: Assessing small subunit rRNA
630 primers for marine microbiomes with mock communities, time series and global field samples, Environ.
631 Microbiol., 18, 1403–1414, https://doi.org/10.1111/1462-2920.13023, 2016.

632 Park, J., Durham, B. P., Key, R. S., Groussman, R. D., Pinedo-Gonzalez, P., Hawco, N. J., John, S. G.,
633 Carlson, M. C. G., Lindell, D., Juranek, L., Ferrón, S., Ribalet, F., Armbrust, E. V., Ingalls, A. E., and Bundy,
634 R. M.: Siderophore production and utilization by microbes in the North Pacific Ocean, bioRxiv,
635 2022.02.26.482025, https://doi.org/10.1101/2022.02.26.482025, 2022.

Park, J., Durham, B. P., Key, R. S., Groussman, R. D., Bartolek, Z., Pinedo-Gonzalez, P., Hawco, N. J., John, S. G., Carlson, M. C. G., and Lindell, D.: Siderophore production and utilization by marine bacteria in the North Pacific Ocean, Limnol. Oceanogr., 68, 1636–1653, 2023.

Quast, C., Pruesse, E., Yilmaz, P., Gerken, J., Schweer, T., Yarza, P., Peplies, J., and Glöckner, F. O.: The SILVA ribosomal RNA gene database project: Improved data processing and web-based tools, Nucleic Acids Res., 41, 590–596, https://doi.org/10.1093/nar/gks1219, 2013.

Reitz, Z. L., Butler, A., and Medema, M. H.: Automated genome mining predicts combinatorial diversity and taxonomic distribution of peptide metallophore structures, bioRxiv, 15–20, https://doi.org/https://doi.org/10.1101/2022.12.14.519525, 2022.

Resing, J. a., Sedwick, P. N., German, C. R., Jenkins, W. J., Moffett, J. W., Sohst, B. M., and Tagliabue, A.: Basin-scale transport of hydrothermal dissolved metals across the South Pacific Ocean, Nature, 523, 200–203, https://doi.org/10.1038/nature14577, 2015.

Rizzi, A., Roy, S., Bellenger, J. P., and Beauregard, P. B.: Iron homeostasis in Bacillus subtilis requires siderophore production and biofilm formation, Appl. Environ. Microbiol., 85, https://doi.org/10.1128/AEM.02439-18, 2019.

Ruttkies, C., Schymanski, E. L., Wolf, S., Hollender, J., and Neumann, S.: MetFrag relaunched: incorporating strategies beyond in silico fragmentation, J. Cheminform., 8, 1–16, https://doi.org/10.1186/s13321-016-0115-9, 2016.

Sander, S. G. and Koschinsky, A.: Metal flux from hydrothermal vents increased by organic complexation, Nat. Geosci., 4, 145–150, https://doi.org/10.1038/ngeo1088, 2011.

Sandy, M. and Butler, A.: Microbial iron acquisition: marine and terrestrial siderophores., Chem. Rev., 109, 4580–95, https://doi.org/10.1021/cr9002787, 2009.

Santoro, A. E., Casciotti, K. L., and Francis, C. A.: Activity, abundance and diversity of nitrifying archaea and bacteria in the central California Current, Environ. Microbiol., 12, 1989–2006, https://doi.org/10.1111/j.1462-2920.2010.02205.x, 2010.

Sheik, C. S., Anantharaman, K., Breier, J. A., Sylvan, J. B., Edwards, K. J., and Dick, G. J.: Spatially resolved sampling reveals dynamic microbial communities in rising hydrothermal plumes across a back-arc basin., ISME J., 9, 1434–45, https://doi.org/10.1038/ismej.2014.228, 2015.

Slagter, H. A., Laglera, L. M., Sukekava, C., and Gerringa, L. J. A.: Fe-Binding Organic Ligands in the Humic-Rich TransPolar Drift in the Surface Arctic Ocean Using Multiple Voltammetric Methods, J. Geophys. Res. Ocean., 124, 1491–1508, https://doi.org/10.1029/2018JC014576, 2019.

Sorokina, M., Merseburger, P., Rajan, K., Yirik, M. A., and Steinbeck, C.: COCONUT online: Collection of Open Natural Products database, J. Cheminform., 13, 1–13, https://doi.org/10.1186/s13321-020-00478-9, 2021.

Stephens, B. M., Opalk, K., Petras, D., Liu, S., Comstock, J., Aluwihare, L. I., Hansell, D. A., and Carlson, C. A.: Organic Matter Composition at Ocean Station Papa Affects Its Bioavailability, Bacterioplankton Growth Efficiency and the Responding Taxa, Front. Mar. Sci., 7, https://doi.org/10.3389/fmars.2020.590273, 2020.

Sumner, L. W., Amberg, A., Barrett, D., Beale, M. H., Beger, R., Daykin, C. A., Fan, T. W.-M., Fiehn, O., Goodacre, R., Griffin, J. L., Hankemeier, T., Hardy, N., Harnly, J., Higashi, R., Kopka, J., Lane, A. N., Lindon, J. C., Marriott, P., Nicholls, A. W., Reily, M. D., Thaden, J. J., and Viant, M. R.: Proposed minimum reporting standards for chemical analysis, Metabolomics, 3, 211–221, https://doi.org/10.1007/s11306-007-0082-2, 2007.

Tagliabue, A., Bowie, A. R., Boyd, P. W., Buck, K. N., Johnson, K. S., and Saito, M. A.: The integral role

of iron in ocean biogeochemistry, Nature, 543, 51–59, https://doi.org/10.1038/nature21058, 2017.

Toner, B. M., Fakra, S. C., Manganini, S. J., Santelli, C. M., Marcus, M. a., Moffett, J. W., Rouxel, O., German, C. R., and Edwards, K. J.: Preservation of iron(II) by carbon-rich matrices in a hydrothermal plume, Nat. Geosci., 2, 197–201, https://doi.org/10.1038/ngeo433, 2009.

Tortell, P. D., Maldonado, M. T., and Price, N. M.: The role of heterotrophic bacteria in iron-limited ocean ecosystems, Nature, 383, 330–332, https://doi.org/10.1038/383330a0, 1996.

Vraspir, J. M. and Butler, A.: Chemistry of marine ligands and siderophores., Ann. Rev. Mar. Sci., 1, 43–63, https://doi.org/10.1146/annurev.marine.010908.163712, 2009.

Wang, H., Wang, W., Liu, M., Zhou, H., Ellwood, M. J., Butterfield, D. A., Buck, N. J., and Resing, J. A.: Iron ligands and isotopes in hydrothermal plumes over backarc volcanoes in the Northeast Lau Basin, Southwest Pacific Ocean, Geochim. Cosmochim. Acta, 336, 341–352, 2022.

Waska, H., Koschinsky, A., Ruiz Chancho, M. J., and Dittmar, T.: Investigating the potential of solid-phase extraction and Fourier-transform ion cyclotron resonance mass spectrometry (FT-ICR-MS) for the isolation and identification of dissolved metal-organic complexes from natural waters, Mar. Chem., 173, 78–92, https://doi.org/10.1016/j.marchem.2014.10.001, 2015.

Whitby, H., Planquette, H., Cassar, N., Bucciarelli, E., Osburn, C. L., Janssen, D. J., Cullen, J. T., González, A. G., Völker, C., and Sarthou, G.: A call for refining the role of humic-like substances in the oceanic iron cycle, Sci. Rep., 10, 6144, 2020.

Whitby, H., Park, J., Shaked, Y., Boiteau, R. M., Buck, K. N., and Bundy, R. M.: New insights into the organic complexation of bioactive trace metals in the global ocean from the GEOTRACES era, Oceanography, 37, 142–155, 2024.

Yücel, M., Gartman, A., Chan, C. S., and Luther, G. W.: Hydrothermal vents as a kinetically stable source of iron-sulphide-bearing nanoparticles to the ocean, Nat. Geosci., 4, 367–371, https://doi.org/10.1038/ngeo1148, 2011.

.

Figures and Tables

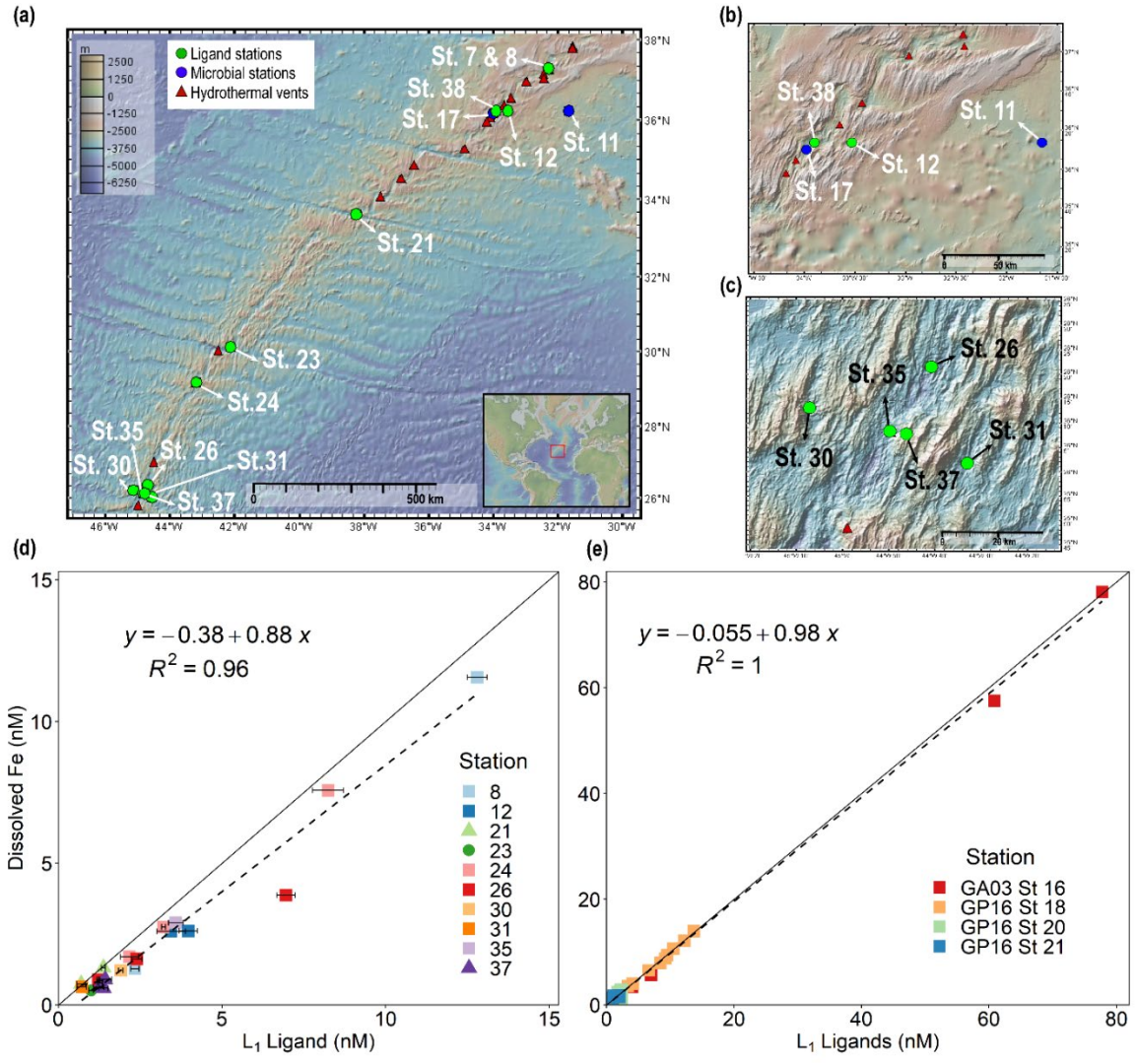

Figure 1. Dissolved iron is strongly correlated with L_1 iron-binding ligands in diverse hydrothermal systems. (a) Station map showing the 11 sites investigated along the MAR. Known hydrothermal vents are marked as red triangles(Beaulieu and Szafrański, 2020). Two expanded inset maps for (b) Rainbow and (c) TAG hydrothermal vent fields. For additional information about vent site characteristics refer to **Table 1**. (d) dFe versus L_1 iron-binding ligands at each vent site in this study showing a ~1:1 correlation (m= 0.88, R^2 = 0.96) with dFe in neutrally-buoyant plumes along the MAR. (e) dFe versus L_1 ligands from previous studies over the ridge axis and ~80 km from ridge axis in the Southern East Pacific Rise hydrothermal plume(Buck et al., 2018), and over TAG hydrothermal vent field(Buck et al., 2015). The solid black lines in (d) and (e) are the 1:1 ratio line between dFe and ligand concentrations, and dashed lines show the linear regression for the corresponding data. Square symbols refer to spreading centers, triangles refer to fracture zones, and

719 circles refer to alkaline vents. Error bars represent the 95% confidence interval of the data fit as calculated
720 by ProMCC(Omanović et al., 2015). The map was created using GeoMapApp version 3.6.14.
721
722

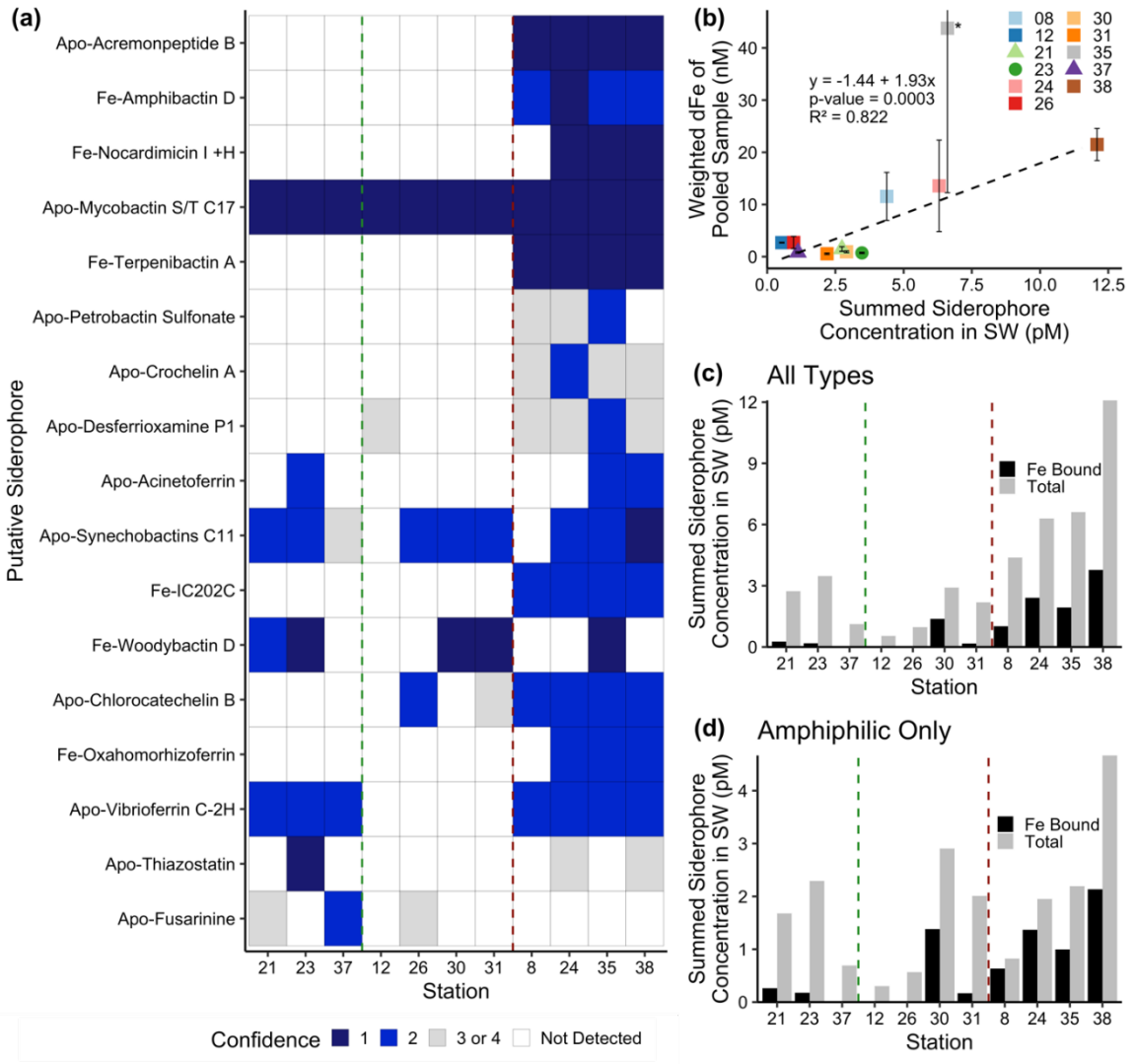

Figure 2. **Siderophore presence in hydrothermal plumes along the MAR.** (a) Heat map of confidence levels 1-2 (blue gradient, 1 = highest confidence). Gray boxes indicate a detection with lower confidence (see Methods), and white boxes indicate no detection at those sites. The y-axis is ordered from top to bottom in terms of descending mass of the apo (without Fe) form of the siderophore. (b) Model II ordinary least squares regression on dFe versus summed siderophore concentrations (of detections in Fig. 2b), calculated from peak areas, at each site. Since the siderophore analysis was performed on pooled samples, the dFe values in the regression are weighted values based on measured dFe and volume of each constituent of the pooled sample. The vertical error bars represent the standard deviation of dFe of the constituents. TAG (St. 35) — denoted by the asterisk — was not included in the regression due to its large range of dFe values and outlier behavior. (c-d) Fe bound versus total summed concentration of (c) all types of siderophores and (d) amphiphilic siderophores at each station. The vertical green lines separate fracture/diffuse sites from off-axis sites and vertical red lines separate off-axis from on-axis sites as defined in Table 1. Symbols follow Fig. 1.

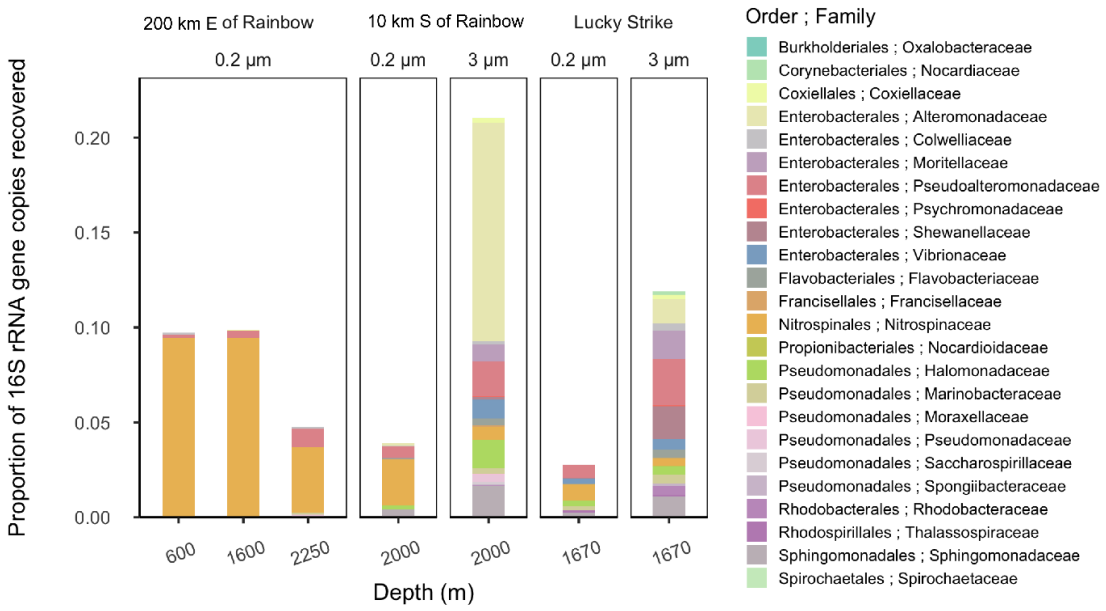

738
739

740 **Figure 3. Relative abundance of putative siderophore-producing taxa.** Bar height indicates the proportion
741 of 16S rRNA genes recovered in each sample, separated by depth from water surface, filter size fraction, and
742 site location. Colors correspond to taxonomy. Genera found in MAR vent microbial communities with
743 members in the antiSMASH database predicted to produce siderophores are depicted at the family level.
744

745 **Table 1. Characteristics of sample locations along the Mid Atlantic Ridge.**

Vent Names	Abbr.	Station	Geology	Host rock	Vent type	Spreading rate (mm/yr)	Summed putative siderophore concentration (pM)	Summed Siderophore concentration/ L_1 ligand (%)*
Lucky Strike	LS	7/8	Spreading Center	gabbro	Black smoker	20.2	4.38	0.034-0.19
33 km E of Rainbow	CER	12	Spreading Center	-	-	-	0.537	0.013-0.017
Rainbow	R	38	Spreading Center	ultramafic	Black smoker	20.6	12.1	*n.a.*
Hayes Fracture Zone	HFZ	21	Fracture Zone	peridotites/gabbro	-	21.2	2.74	0.20-0.39
Lost City	LC	23	Fracture Zone	ultramafic/gabbro	Alkaline	22.6	3.47	0.27-0.35
Broken Spur	BS	24	Spreading Center	gabbro	Black smoker/diffuse	22.9	6.30	0.07-0.29
29 km N of TAG	CNT	26	Spreading Center	-	-	-	0.968	0.014-0.079
30 km W of TAG	CWT	30	Spreading Center	-	-	-	2.91	0.15
30 km E of TAG	CET	31	Spreading Center	-	-	-	2.19	0.31

Trans-Atlantic Geotraverse	TAG	35	Spreading Center	gabbro	Black smoker	23.6	6.61	0.18
Low Temp Slope	LTS	37	-	-	Diffuse fluids	-	1.13	0.079-0.087

Spreading rates along the Mid-Atlantic Ridge were gathered from the Interridge Database v3.4. Host rock groups were determined from previously discussed classifications(Bazylev, 1997; Kelley and Shank, 2010). Off-axis sites –33 km E of Rainbow, 29 km N of TAG, 30 km E of TAG, and 30 km W of TAG– were far-field locations of their respective vent field. Low Temp Slope was a diffuse-dominated site that was sampled for the first time as a part of this study. Summed putative siderophore concentrations and the percent of L_1 ligand are reported for compounds detected with at least confidence level 1 and 2 at one site. These values do not take into account typical extraction efficiencies of ENV columns for Fe-binding organics. Average L_1 ligand and siderophore concentrations can be viewed in **Table S3** and concentrations for individual siderophores can be observed in **Table S5**.

*The siderophore sample at each site was pooled from ligand samples, so the percentage of siderophores in the L_1 pool is presented as a range based on the range of L_1 concentrations at each site.

n.a.= unable to be determined

- = unknown

746

747